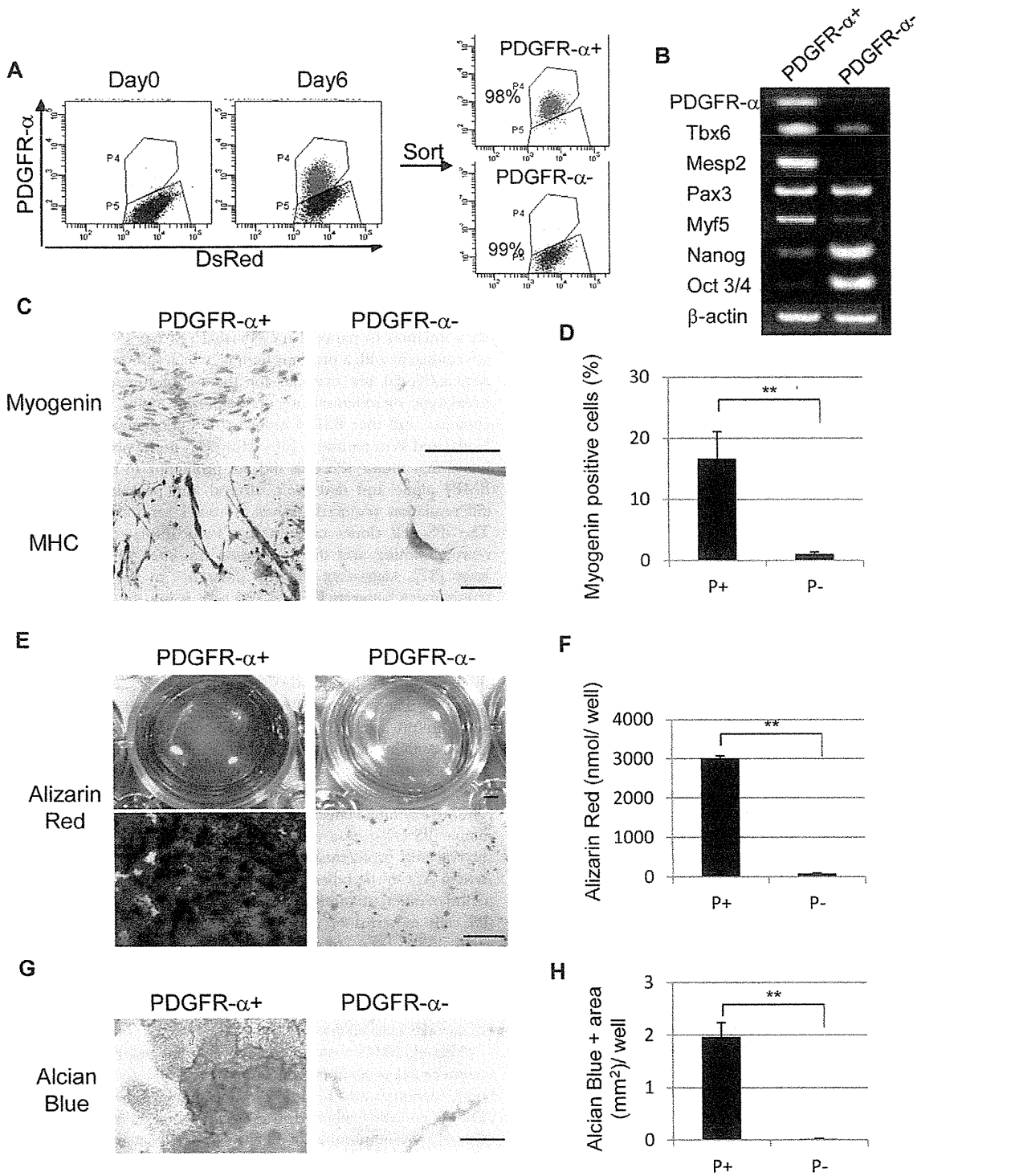

Figure 4. Differentiation potential of mouse iPS cell-derived paraxial mesodermal progenitors *in vitro*. (**A**) On day 6, differentiated iPS cells were sorted into PDGFR-α$^+$ and PDGFR-α$^-$ populations. (**B**) Gene expression profile for mesodermal and undifferentiated markers in PDGFR-α$^+$ and PDGFR-α$^-$ populations. (**C**) *In vitro* myogenic differentiation of sorted cells 7 days after differentiation. The differentiation of PDGFR-α$^+$ cells, but not PDGFR-α$^-$ cells, into mature myocytes is shown as myogenin$^+$ cells with brown nuclear staining (upper panels) or as myosin heavy chain (MHC)-positive cells with brown cytosolic staining (lower panels). (**D**) The ratio of myogenin$^+$ cells to the total number of cells that were Giemsa-positive in each well was counted. Approximately 16% of PDGFR-α$^+$ cells were myogenin$^+$ (n = 3). (**E**) *In vitro* osteogenesis of differentiated mouse iPS cells 28 days after osteocytic induction. The PDGFR-α$^+$ population differentiated into osteocytes, producing an Alizarin Red-positive calcium matrix. The PDGFR-α$^-$ population showed limited osteogenic potential, as indicated by faint calcium deposits (n = 3, each). (**F**) Quantification of Alizarin Red dyes in an osteogenic differentiation culture (n = 3). (**G**) *In vitro* chondrogenesis of differentiated mouse iPS cells 21 days after chondrocytic induction. The

PDGFR-α$^+$ population gave rise to Alcian Blue-positive chondrocytes. (n = 3, each) (**H**) Quantification of Alcian Blue positive area in a chondrogenic differemtiation culture (n = 3). The bars in (**C**) and (**G**) represent 100 μm, the bar in (**E upper**) represents 2 mm and the bar in (**E lower**) represents 200 μm. **p<0.01 between selected two samples.
doi:10.1371/journal.pone.0047078.g004

(PDGFR-α single positive; PSP), PDGFR-α$^-$/KDR$^+$ (KDR single positive; KSP), and PDGFR-α$^-$/KDR$^-$ (double negative; DN) (Fig. 6B). As shown in Fig. 6C, the proportion of each fraction was similar in 2 distinct human iPS cell clones. Approximately one third of cells expressed PDGFR-α, and the PSP population rose to around 20% of cells in both iPS cell clones.

Previously, we reported that while the PSP population displayed paraxial mesodermal characteristics, the DP population displayed immature mesodermal characteristics during mouse ES cell differentiation [8]. Therefore, to assess the characteristics of each cell population, we performed quantitative PCR analysis of developmental markers (Fig. 6D). The expression levels of PDGFR-α and KDR were analyzed to confirm the purity of each FACs-sorted population. In both iPS cell clones, the paraxial mesodermal markers *Tbx6* and *Mesp2* were dominantly expressed in the PSP population. In contrast, the neuronal marker *Pax6* was specifically detected in the DN population, suggesting that neural lineage cells were negatively selected by the two mesodermal markers. Taken together, the gene expression profile indicates that the PSP population isolated after differentiation of human iPS cells displays paraxial mesodermal characteristics.

The PDGFR-α$^+$/KDR$^-$ Population Differentiated from Human iPS Cells Exhibits Paraxial Mesodermal Characteristics with Differentiating Potentials into Skeletal Myocytes, Osteocytes, and Chondrocytes *in vitro*

Next, we investigated the *in vitro* differentiation potential of the PSP population derived from human iPS cells to paraxial mesoderm descendants, such as myocytes, osteocytes, and chondrocytes. Differentiated human iPS cells at Day6 were separated into 4 fractions–DP, DN, PSP and KSP– by FACS Aria and re-cultured for further differentiation. In osteogenic differentiation culture, Alizarin Red-positive calcium matrix was dominantly detected in the culture of PSP population, indicating that PSP cells have enough potential to differentiate into osteocytes (n = 3) (Fig. 7A). Quantification of total amount of Alizarin Red dyes in a well demonstrated that osteogenic cells were mainly contained within PSP population (Fig. 7B). In chondrogenic differentiation culture, both PSP population and DP population gave rise to Alcian Blue-positive chondrocytes (n = 3) (Fig. 7C). Quantification of Alcian Blue-positive area in a well showed that chondrogenic progenitors were mainly contained in PSP population (Fig. 7D). In myogenic differentiation culture, MHC-positive mature myocytes were selectively detected in the PSP population (n = 3) (Fig. 7E and 7F). These results indicate that PSP cells derived from human iPS cells have the potential to differentiate into three paraxial mesodermal descendants *in vitro*, including skeletal myocytes, osteocytes, and chondrocytes. Thus, these results suggest that the human iPS cell-derived PSP cells represent paraxial mesodermal progenitors.

Discussion

Since Yamanaka and Takahashi first reported the generation of pluripotent ES cell-like cells–induced pluripotent stem (iPS) cells–from mouse fibroblasts by unique gene transfer-based nuclear reprogramming technology, many researchers have compared the similarities and differences between ES and iPS cells with respect to their pluripotency, undifferentiated states, genetic or epigenetic regulations, and differentiation potentials. For lateral mesodermal differentiation into cardiomyocytes, endothelial cells, and hematopoietic cells, mouse iPS cells have almost identical differentiation potential to mouse ES cells. In the present study, we demonstrated a potential of mouse ES and iPS cells for paraxial mesodermal differentiation, with the exception of the requirement of Activin A during iPS cell differentiation under serum-free conditions.

Previously, we demonstrated that BMP4 treatment was sufficient to promote commitment of mouse ES cells to the early primitive streak-type mesodermal lineage [14] and further their differentiation to paraxial mesodermal cell types. These findings are consistent with a previous finding, which showed that Wnt and Activin/Nodal are essential for the establishment of primitive streak-type mesodermal precursors during mouse ES cell differentiation and that BMP4 induces the endogenous activation of Nodal and Wnt pathways [36]. However, in the present study, we found that mouse iPS cells did not proliferate in the presence of BMP4 alone and that their survival and paraxial mesodermal differentiation required Activin A under serum-free conditions. The iPS cell clones used in this study display near complete reprogramming and show germline transmission in a chimeric assay [37], suggesting that the difference in the growth factor requirement between ES and iPS cells is not due to incomplete reprogramming of iPS cells. We rather consider that the requirement of Activin A by iPS cells is due to their intrinsic characteristics. More than 80% of the mouse iPS cells died by apoptosis in 24 hours after serum-free differentiation without Activin A, whereas only 10% of mouse ES showed apoptosis in the same culture condition. Mouse ES cells activate endogenous Nodal/Activin signaling in an autocrine fashion to proliferate under serum-free conditions [38]. Based on the finding that mouse iPS cells express less transcripts of the Nodal gene than mouse ES cells, we examined effects of Activin A on the serum-free culture of mouse iPS cells. As a result, we attained prominently enhanced survival and proliferation of mouse iPS cells in the presence of Activin A. On the other hand, the response to Activin A in early period of differentiation was quite identical between mouse ES and iPS cells in terms of increased expression of mesoendodermal genes [39]. Thus, mouse iPS cells are likely less capable of activating Nodal/Activin signaling, which is essential for their survival rather than for differentiation. Severe conditions, such as serum-free monolayer culture, should uncover differences between ES and iPS cells efficiently.

Although BMP4 was not essential for the induction of paraxial mesodermal progenitors from mouse iPS cells in the presence of both Activin A and LiCl and did not influence the proportion of PDGFR-α$^+$ cells generated in cell culture, the addition of BMP4 affected the composition of PDGFR-α$^+$ cells in a concentration-dependent manner. In particular, 10 ng/ml of BMP4 enhanced expression of paraxial mesodermal markers, whereas higher doses of BMP4 inhibited the expression of the myogenic marker *Myf5*, as consistent with previous reports [26]. In contrast, the addition of LiCl, which activates Wnt signaling via inhibition of GSK3β, dramatically increased the proportion of PDGFR-α$^+$ cells in serum-free culture. Mesodermal gene expression patterns in the presence or absence of LiCl were almost identical, with the exception of elevated *Myf5* expression in the presence of LiCl. Therefore, these results suggest that Wnt signaling promotes

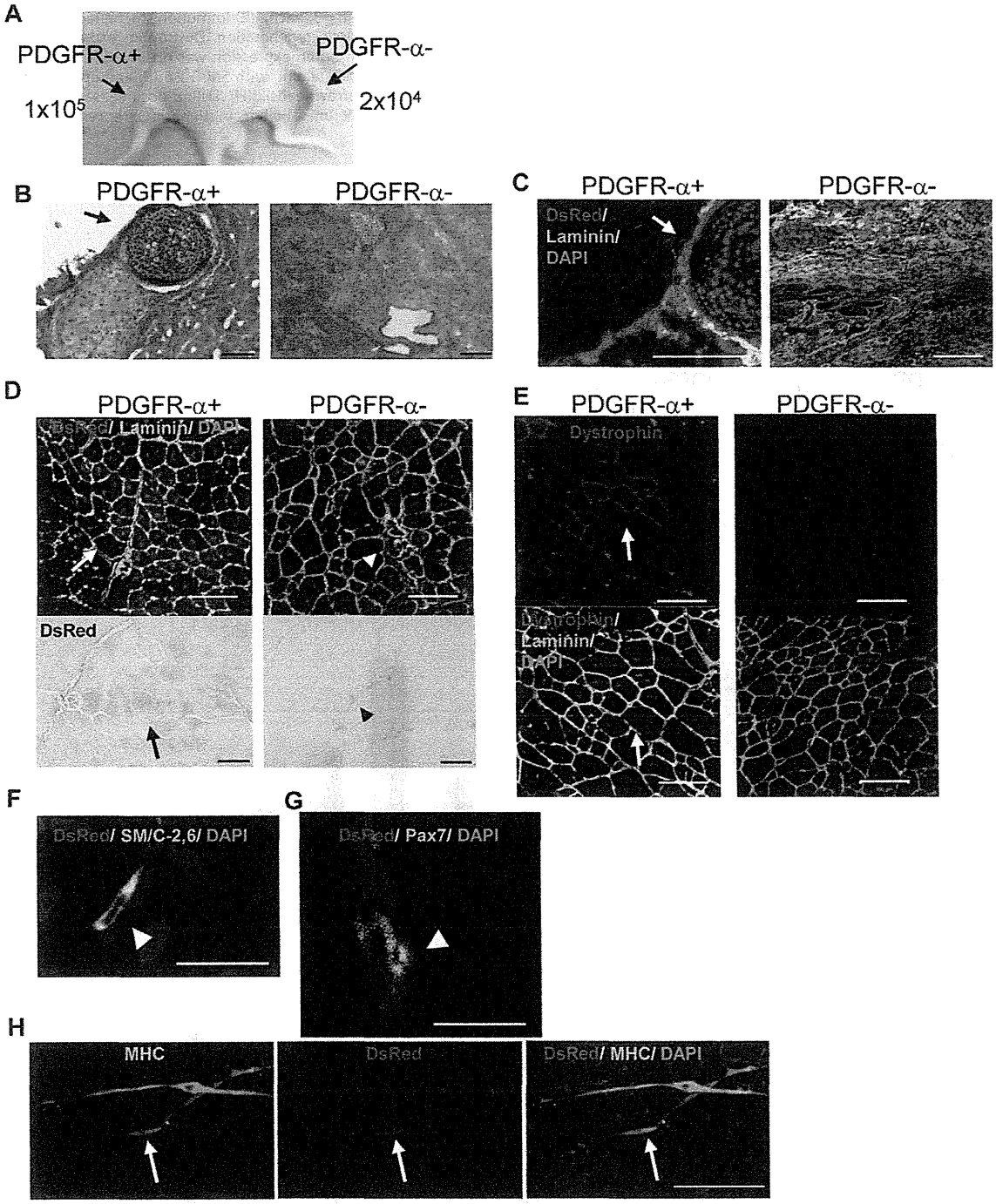

Figure 5. Differentiation potential of mouse iPS cell-derived paraxial mesodermal progenitors toward chondrocytes and myocytes *in vivo*. (**A**) Differentiated iPS cells were sorted into PDGFR-α^+ and PDGFR-α^- populations on day 6. The resulting sorted cells were intramuscularly transplanted into the tibia anterior (TA) muscles of nude mice. Tumor formation was detected in muscle engrafted with the PDGFR-α^- population (n = 4). (**B**, **C**) The PDGFR-α^+ population differentiated into chondrocytes *in vivo*. The iPS-DsRed cell-derived PDGFR-α^+ or PDGFR-α^- populations within Matrigel were grafted into TA muscle. The PDGFR-α^- population formed a teratoma (**B**, right), and the PDGFR-α^+ population formed ectopic cartilage (**B**, left; arrow). (**C**) The teratomas and ectopic cartilage were derived from engrafted cells that expressed DsRed. (**D**) Differentiation potential of the PDGFR-α^+ population toward skeletal muscle *in vivo*. The iPS-DsRed cell-derived PDGFR-α^+ or PDGFR-α^- populations were recultured on thermoreactive dishes for 24 h and harvested without enzymatic treatment. The harvested cells were directly transplanted into TA muscles of nude mice (n = 3, each). Immunohistochemical staining with anti-DsRed antibody was performed to detect engrafted cells. Upper panels: DsRed positive engrafted cells derived from PDGFR-α^+ population fused with host myofibers (white arrow), while DsRed positive engrafted cells derived from PDGFR-α^- population located in interstitial area of host muscle (white arrowhead). Lower panels: DsRed expression was confirmed by HRP-based immunohistochemistry (black arrow and black arrowhead). (**E**–**G**) The PDGFR-α^+ population differentiated to form dystrophin-positive muscle fibers

in DMD-null mice. The harvested cells were directly transplanted into TA muscles of DMD-null mice (n = 3, each). (**E**) Immunohistochemical staining with anti-dystrophin antibody was performed to assess the contribution of engrafted cells to muscle regeneration. Dystrophin expression was detected at the injected site of PDGFR-α^+ population engrafted muscle (white arrow), while no Dystrophin expression was observed in PDGFR-α^- population engrafted muscle. (**F, G**) To assess differentiation into satellite cells, immunohistochemical staining with SM/C-2.6 (**F**) and anti-Pax7 (**G**) antibodies was performed. DsRed-positive cells were able to differentiate into satellite cells (arrowheads). (**H**) DsRed-positive satellite cells differentiated into mature myocytes *in vitro* (arrow). The bars in (**B**), (**C**), (**D**), (**E**), and (**H**) represent 100 μm. The bars in (**F**) and (**G**) represent 10 μm.
doi:10.1371/journal.pone.0047078.g005

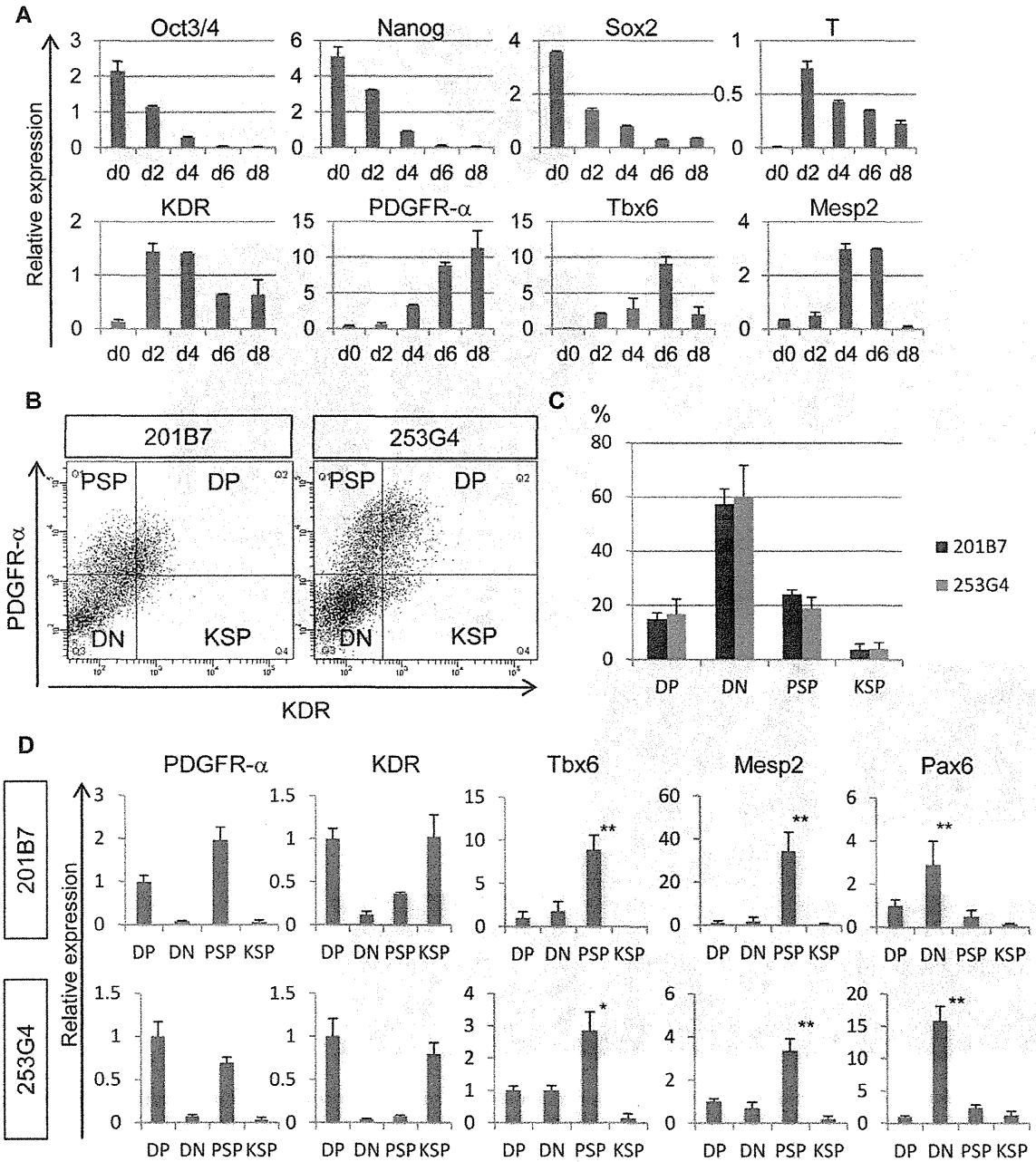

Figure 6. Modeling paraxial mesodermal differentiation of human iPS cells. (**A**) Time course of gene expression profile during differentiation of human iPS cells. (**B**) Expression profile of PDGFR-α and KDR in differentiated human iPS cells on day 6. DP, double-positive population; DN, double-negative population; PSP, PDGFR-α single-positive population; KSP, KDR single-positive population. (**C**) Proportion of each fractionated population of differentiated human iPS cells on day 6 (n = 3). About one third of cells were PDGFR-α positive, and around 20% of the total cells were classified in the PSP population. (**C**) Gene expression profiles of each population after differentiation of human iPS cells. *Tbx6* and *Mesp2* were dominantly expressed in the PSP population. *p<0.05, **p<0.01 PSP versus the other samples (Tbx6 and Mesp2). **p<0.01 DN versus the other samples (Pax6).
doi:10.1371/journal.pone.0047078.g006

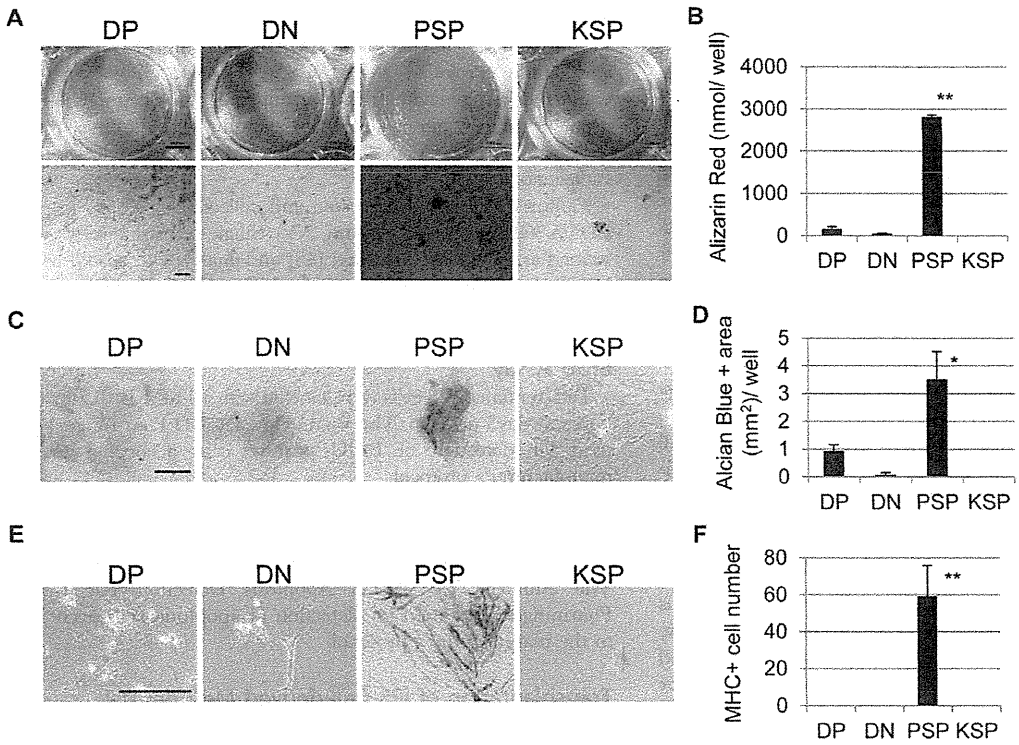

Figure 7. Differentiation potential of human iPS cell-derived mesodermal populations *in vitro*. (**A**) *In vitro* osteogenesis of differentiated human iPS cells 28 days after osteocytic induction. On day 6, differentiated human iPS cells were sorted into DP, DN, PSP and KSP populations. The PSP population differentiated into osteocytes, producing an Alizarin Red-positive calcium matrix. The DP population showed low osteogenic potential, as indicated by mild calcium deposits (n = 3, each). The DN and KSP populations had very low osteogenic potentials (n = 3, each). (**B**) Quantification of Alizarin Red dyes in an osteogenic differentiation culture (n = 3). (**C**) *In vitro* chondrogenesis of differentiated mouse iPS cells 21 days after chondrocytic induction. The PSP and DP populations gave rise to Alcian Blue-positive chondrocytes, while the DN and KSP populations had very low chondrogenic potentials. (n = 3, each) (**D**) Quantification of Alcian Blue positive area in a chondrogenic differemtiation culture (n = 3). (**E**) *In vitro* myogenic differentiation of sorted cells 14 days after differentiation. The differentiation of PPS cells, but not the other cells, into mature myocytes is shown as MHC^+ cells with brown cytosolic staining (n = 3, each). (**F**) The number of MHC^+ cells in a myogenic differentiation culture was counted (n = 3). The bar in (**A upper**) represents 4 mm, the bar in (**A lower**), (**C**) and (**E**) represents 100 μm. *$p<0.05$, **$p<0.01$ PSP versus the other samples.
doi:10.1371/journal.pone.0047078.g007

paraxial mesodermal differentiation, particularly toward myogenic differentiation, during mouse iPS cell differentiation.

Although some differences in growth factor requirement between mouse ES cell and iPS cells were observed, the PDGFR-α^+ population derived from mouse iPS cells was almost identical to that of ES cells with respect to their differentiation potential toward paraxial mesoderm descendants, such as osteocytes, chondrocytes, and myocytes. Particularly for myogenic differentiation, the iPS cell-derived PDGFR-α^+ population contains myogenic progenitor cells that can give rise to satellite cells and contribute to regeneration of impaired muscle in DMD-null mice by the production of dystrophin. However, since the same PDGFR-α^+ population induces ectopic cartilage formation, even following engraftment into muscle with Matrigel, it will be necessary to further dissect this population into committed myogenic and chondrogenic populations by using other markers.

In human iPS cell differentiation, PDGFR-α has been recognized as a segregation marker for isolating KDR^+/PDGFR-α^- hematopoietic progenitors and KDR^+/PDGFR-α^+ cardiac progenitors among KDR^+ mesodermal progenitors [40,41]. In the present study, we demonstrated that PDGFR-α can be effectively used in combination with KDR negative selection to isolate paraxial mesodermal progenitor cells from human iPS cells after differentiation as well as in a mouse ES/iPS cell differentiation system. The human iPS cell-derived PDGFR-α^+/KDR^- cells named PDGFR-α single positive (PSP) population significantly exhibited higher differentiation potentials to paraxial mesodermal descendants such as osteocytes, chondrocytes and myocytes than the other three populations. Whereas the protocols for osteogenic and chondrogenic differentiation of human iPS cells were similar to the protocols of mouse iPS cell, myogenic differentiation had to be customized for human iPS cells. The human iPS cell-derived PSP population did not differentiate to myocytes in the presence of serum or KSR, but did differentiate to myocytes in serum-free condition with additional supplement of LiCl and a TGF-β signal inhibitor SB-431542 [42]. However, many other cell types were still observed in this myogenic differentiation culture and efficiency of myogenesis still remained low. It will be necessary to explore further purification of committed myogenic lineage from PSP population by using other markers.

Finally, the isolation of paraxial mesodermal progenitors during human iPS cell differentiation will be a first step to purify osteogenic, chondrogenic and myogenic progenitors by their segregation from residual undifferentiated stem cells for use in stem cell therapies to treat diseased bone, cartilage, and muscle.

Materials and Methods

In vitro Cell Culture and iPS Cell Differentiation

Mouse iPS-MEF-Ng-20D-17 (iPS-Ng), iPS-MEF-Ng-492B-4 (iPS-plasmid), and iPS-TTF-DsRed-256H-18 (iPS-DsRed) iPS cells were kindly provided by Dr. S. Yamanaka and maintained as described previously [5,43,44]. Mouse fibroblasts were obtained from mouse tail-tip or embryo in strict accordance with the recommendations in the Regulation on Animal Experimentation at Kyoto University, and the protocol to produce the fibroblasts was approved by the Animal Research Committee of Kyoto University. For paraxial mesoderm differentiation, $1.6–2.4\times10^5$ mouse iPS cells were plated onto a 6-cm dish coated with type IV collagen (Nitta Gelatin, Inc.) and differentiated in serum-free culture medium (SF-O3; Sanko Junyaku) supplemented with 0.2% bovine serum albumin (BSA), 0.1 mM 2-mercaptoethanol (2-ME), 5 ng/ml recombinant human Activin A (Peprotech), 10 ng/ml recombinant human IGF-1 (Peprotech), and 10 ng/ml recombinant human BMP4 (R&D Systems Inc., Minneapolis). After 3 days of culture, the medium was replaced with SF-O3 supplemented with 0.2% BSA, 0.1 mM 2-ME, 5 mM LiCl (Nacalai Tesque), and 10 ng/ml recombinant mouse Shh (R&D). Following 6 days of culture, paraxial mesodermal progenitor cells were obtained as PDGFR-α^+ cells. For osteocytic and chondrocytic induction, paraxial mesodermal progenitor cells were sorted as described below and recultured as previously described [8]. Similarly, for myogenic differentiation, paraxial mesodermal progenitor cells were sorted as described below and recultured as described previously [14].

Human iPS cells (201B7 and 253G4) were also kindly provided by Dr. S. Yamanaka and maintained as previously described [2]. Human dermal fibroblasts used for generating 201B7 and 253G4 were purchased from Cell Applications, Inc. All human iPS cells were established according to procedures approved by Ethics Committee on Human Stem Cell Research of the Institute for Frontier Medical Sciences, Kyoto University. For mesodermal differentiation, feeder cells were depleted by treatment with 0.25% trypsin (Invitrogen), 0.1 mg/ml collagenase IV (Invitrogen), 1 mM $CaCl_2$ (Nacalai Tesque), and 20% Knockout serum replacement (KSR; Invitrogen) at room temperature (RT) for 2 min. After feeder cell depletion, human iPS cells were washed twice with PBS(-), and an appropriate volume of differentiation medium, [alpha-minimum essential medium (αMEM; Nacalai Tesque) supplemented with 5% KSR and 0.1 mM 2-ME] was added to the culture dish. Human iPS cells were detached by scraping and dissociated into small clusters by pipetting, which were plated onto dishes coated with type I collagen (passage ratio, 1:2). Human iPS cells were cultured in differentiation medium at 37°C with 5% CO_2, and the differentiation medium was changed every 2 days. For osteocytic and chondrocytic induction, fractionated cells were sorted as described below and recultured as previously described [8]. For myogenic induction, the fractionated cells were sorted as described below and were re-cultured on collagen type I coated 24-well trays (AGC TECHNO GLASS) in SF-O3 with 5 mM LiCl, 10 ng/mL IGF-1, 10 ng/mL hepatocyte growth factor (HGF) (R&D systems) and 10 ng/mL basic fibroblast growth factor (bFGF) (Wako). Three days after re-culture, the medium was changed again to SF-O3 with 5 mM LiCl, 10 ng/mL IGF-1 and 5 μM SB-431542 (Stemgent Inc.). Four days later, the medium was changed again to SF-O3 with 10 ng/mL IGF-1, 5 μM SB-431542 and 10 ng/mL HGF and the cells were cultured for seven days.

Antibodies, Cell Staining, FACS Analyses, and Cell Sorting

The rat monoclonal antibody (MAb) APA5 (anti-PDGFR-α) [9] was kindly provided by Dr. S. Nishikawa. Phycoerythrin-conjugated streptavidin (BD Pharmingen, San Diego, CA) was used to detect biotinylated-APA5 antibody. Allophycocyanin (APC)-conjugated AVAS12 (Anti-Flk-1) MAb was purchased from Biolegend.

Cultured cells were harvested and collected in 0.05% trypsin-EDTA (GIBCO, Grand Island, NY). Single-cell suspensions were stained as previously described [45] and analyzed or sorted with a FACS Aria (Becton, Dickinson and Company, Franklin Lakes, NJ).

BrdU Assay

Differentiated iPS cells were labeled with 10 mM BrdU for four hours at day3 or day6. The BrdU Flow kit (BD Pharmingen) was used for detection of BrdU positive cells according to the manufacturer's protocol.

Apoptosis Assay

Differentiated iPS cells were harvested at day1, day3 or day6. The Annexin V : FITC Apoptosis Detection Kit I (BD Pharmingen) was used for detection of apoptotic cells according to the manufacturer's protocol.

Transplantation of iPS Cell-derived Mesodermal Progenitors into Mice

All mouse experiments were carried out according to protocols approved by the Animal Research Committee of Kyoto University. The PDGFR-α^+ and PDGFR-α^- fractions were purified and collected by FACS Aria. Cells were resuspended in Matrigel (Invitrogen) or in αMEM supplemented with 10% fetal bovine serum (FBS; Invitrogen) and 100 μM 2-ME. Alternatively, collected cells were reseeded onto thermo-responsive culture dishes pre-coated with type IV collagen and were cultured in αMEM supplemented with 7% FBS, 10 ng/ml recombinant human IGF-1 and 100 μM 2-ME. Cells were harvested 24 h after reseeding by incubation at RT without enzymatic treatment and were resuspended in the culture media. For intra-muscular transplantation of immunodeficient mice, the tibia anterior (TA) muscle of a KSN nude mouse (Japan SLC, Inc., Hamamatsu, Japan) was treated with Cardiotoxin (CalBiochem) following diethyl ether anesthesia 24 h before transplantation, which consisted of the direct injection of 50 μl of cell suspension into the TA muscle of each mouse. For intra-muscular transplantation of a Duchenne muscular dystrophy (DMD)-model mouse, a DMD-null mouse was totally irradiated with 6 Gy of γ-rays and the TA muscle was treated with Cardiotoxin (CalBiochem) following diethyl ether anesthesia 24 hour before transplantation. For cell transplantation, 50 μl of cell suspension was directly injected into the TA muscle of each mouse. All mice used in this study were humanely sacrificed 28 days after transplantation and tissue samples were collected.

Quantitative RT-PCR Analysis

Total RNA was isolated using Sepazol reagent (Nacalai Tesque) according to the manufacturer's protocol. Residual genomic DNA was digested and removed with DNase I (Invitrogen). First-strand cDNA was synthesized using the Superscript III First-Strand Synthesis System (Invitrogen) for RT-PCR and oligo (dT) 12–18 primers. The cDNA was diluted with DNase-free water at a concentration of 10 ng/μl. Quantitative RT-PCR was performed using the PowerSYBR PCR kit (Applied Biosystems) according to

the manufacturer's instructions and a StepOne thermal cycler (Applied Biosystems). We used the *Rpl13a* and *β-actin* genes as invariant controls for mouse and human samples, respectively. For standardization of mouse iPS cell experiments, cDNA from E13.5 mouse embryo was defined as the control value (1.0). For human iPS cell experiments, we defined the value of the cDNA from a teratoma derived from 201B7 (Fig. 6A), or double positive (DP) (Fig. 6D) as the control value (1.0) for standardization. The primers are listed in Table S1.

Histochemical Staining for Osteogenesis and Chondrogenesis

Alizarin Red and Alcian Blue staining was performed as previously described [46]. Briefly, cultured cells were fixed with 4% paraformaldehyde in PBS for 5 min at RT and subsequently washed twice with PBS for 5 min at RT. For calcium detection, fixed cells were incubated in 1% Alizarin Red S solution (Sigma) for 5 min at RT and subsequently washed 5 times with PBS at RT. For the detection of mucopolysaccharide in cartilage, fixed cells were incubated in 3% acetate solution for 5 min at RT and subsequently incubated in 1% Alcian Blue 8GX (Sigma) and 3% acetate solution for 30 min at RT. Finally, the cells were washed 5 times with 3% acetate solution and twice with PBS.

Immunohistochemistry

Immunohistochemical analyses were performed as previously described [47], and the following antibodies were used: rabbit anti-DsRed (Clontech; 1:5000), mouse anti-myogenin (Santa Cruz Biotechnology, Inc., Santa Cruz, CA; 1:400), rabbit anti-dystrophin (Abcam; 1:200), mouse anti-Pax7 (R&D; 1:100), rat anti-laminin a2 (Alexis; 1:150), rabbit anti-β-catenin (Sigma; 1:500), goat anti-PDGFR-α (R&D; 1:200) and rabbit anti-myosin heavy chain (R&D; 1:400). A rat MAb satellite cell marker, SM/C-2.6 [33], was kindly provided Dr H. Fukada and used at a dilution of 1:400. Horse radish peroxidase (HRP)-conjugated anti-mouse IgG (Chemicon), Alexa 488-conjugated anti-rat IgG (Invitrogen), Alexa 488-conjugated anti-mouse IgG (Invitrogen), Alexa 568-conjugated anti-rabbit IgG (Invitrogen), and Alexa 568-conjugated anti-goat IgG (Invitrogen) were used as secondary antibodies. For detection of Pax7, an anti-Pax7 antibody was directly labeled with Alexa-488 by using the Zenon system (Invitrogen).

Animal Welfare

This study was carried out in strict accordance with the recommendations in the Regulation on Animal Experimentation at Kyoto University. The protocols in this study were approved by the Animal Research Committee of Kyoto University (Protocol number CiRA1-3 to Hidetoshi Sakurai). All injections were performed under anesthesia, and all efforts were made to minimize suffering. Mice were humanely sacrificed prior to tissue collection.

Statistical Analysis

Differences between samples were assessed by using the Student's two-tailed t test for independent samples.

References

1. Takahashi K, Yamanaka S (2006) Induction of pluripotent stem cells from mouse embryonic and adult fibroblast cultures by defined factors. Cell 126: 663–676.
2. Takahashi K, Tanabe K, Ohnuki M, Narita M, Ichisaka T, et al. (2007) Induction of pluripotent stem cells from adult human fibroblasts by defined factors. Cell 131: 861–872.
3. Yu J, Vodyanik MA, Smuga-Otto K, Antosiewicz-Bourget J, Frane JL, et al. (2007) Induced pluripotent stem cell lines derived from human somatic cells. Science 318: 1917–1920.
4. Amabile G, Meissner A (2009) Induced pluripotent stem cells: current progress and potential for regenerative medicine. Trends Mol Med 15: 59–68.

Supporting Information

Figure S1 Responses to Activin A of mouse ES/iPS cells during mesodermal differentiation. (**A**) Apoptosis of differentiated mouse ES cells on D1 assessed by a proportion of Propidium Iodide (PI) positive/AnnexinV positive cell (n = 3). (**B**) Nodal expression of differentiated ES and iPS cells on D1. More Nodal expression was observed in mouse ES cells than mouse iPS cells. (**C**) Expression level of early mesendodermal markers in mouse ES and iPS cells on D3 with (gray bars) or without (black bars) addition of Activin A (n = 3). Activin A treatment significantly activated expression of mesoendodermal genes in both mouse ES and iPS cells. (**D**) Gene expression profiles of PDGFR-α^+ cells in lower dose treatment of Activin A (n = 3). The expression levels of *Tbx6* and *Mesp2* genes were not affected within those concentration of Activin A. *p<0.05, **p<0.01 between selected two samples.
(PDF)

Figure S2 Responses to LiCl and Shh of mouse iPS cells during mesodermal differentiation. (**A, B**) The expression of PDGFR-α in mouse iPS cells after differentiation. The gray bars indicates the percentage of PDGFR-α^+ cells in various concentration of LiCl (**A**) or Shh (**B**) (n = 3, each). We choose suitable dose of LiCl or Shh by the proportion of PDGFR-α^+ cells, as 5 mM LiCl or 10 ng/ml Shh, respectively. (**C**) LiCl acts as an inducer of Wnt signaling. The localization of β-catenin shifted from cytoplasmic region (upper panels) into nucleus (lower panels) after LiCl treatment. (**D**) Proliferation of differentiated mouse iPS cells on D6 assessed by BrdU assay (n = 3). Addition of Shh significantly promoted cell proliferation. (**E**) Apoptosis of differentiated mouse ES cells on D6 assessed by a proportion of PI positive/AnnexinV positive cell (n = 3). Addition of LiCl significantly reduced apoptosis of differentiated iPS cells. *p<0.05, **p<0.01 between selected two samples. The bar represents 50 μm.
(PDF)

Figure S3 Morphology of PDGFR-α positive cells after mesodermal differentiation of mouse iPS cells. PDGFR-α^+ cells (red) are distinguishable by their prominent cellular clumping on D6 differentiation. The bars represent 100 μm.
(PDF)

Table S1 Primes used for RT-PCR. All forward primers are indicated in upper rows, and all reverse primers are indicated in lower rows.
(DOC)

Acknowledgments

We thank Dr. Shinya Yamanaka for providing mouse and human iPS cells. We would also like to thank Dr. T. Sato and Dr. M. Ikeya for valuable scientific discussions.

Author Contributions

Conceived and designed the experiments: HS AS. Performed the experiments: HS YS ES. Analyzed the data: HS YS ES AK AS. Contributed reagents/materials/analysis tools: TN IM HS KH. Wrote the paper: HS AS.

5. Okita K, Hong H, Takahashi K, Yamanaka S (2010) Generation of mouse-induced pluripotent stem cells with plasmid vectors. Nat Protoc 5: 418–428.
6. Nakagawa M, Takizawa N, Narita M, Ichisaka T, Yamanaka S (2010) Promotion of direct reprogramming by transformation-deficient Myc. Proc Natl Acad Sci U S A 107: 14152–14157.
7. Maekawa M, Yamaguchi K, Nakamura T, Shibukawa R, Kodanaka I, et al. (2011) Direct reprogramming of somatic cells is promoted by maternal transcription factor Glis1. Nature 474: 225–229.
8. Sakurai H, Era T, Jakt LM, Okada M, Nakai S, et al. (2006) In vitro modeling of paraxial and lateral mesoderm differentiation reveals early reversibility. Stem Cells 24: 575–586.
9. Kataoka H, Takakura N, Nishikawa S, Tsuchida K, Kodama H, et al. (1997) Expressions of PDGF receptor alpha, c-Kit and Flk1 genes clustering in mouse chromosome 5 define distinct subsets of nascent mesodermal cells. Dev Growth Differ 39: 729–740.
10. Schatteman GC, Morrison-Graham K, van Koppen A, Weston JA, Bowen-Pope DF (1992) Regulation and role of PDGF receptor alpha-subunit expression during embryogenesis. Development 115: 123–131.
11. Nakayama N, Duryea D, Manoukian R, Chow G, Han CY (2003) Macroscopic cartilage formation with embryonic stem-cell-derived mesodermal progenitor cells. J Cell Sci 116: 2015–2028.
12. Winnier G, Blessing M, Labosky PA, Hogan BL (1995) Bone morphogenetic protein-4 is required for mesoderm formation and patterning in the mouse. Genes Dev 9: 2105–2116.
13. Takada S, Stark KL, Shea MJ, Vassileva G, McMahon JA, et al. (1994) Wnt-3a regulates somite and tailbud formation in the mouse embryo. Genes Dev 8: 174–189.
14. Sakurai H, Inami Y, Tamamura Y, Yoshikai T, Sehara-Fujisawa A, et al. (2009) Bidirectional induction toward paraxial mesodermal derivatives from mouse ES cells in chemically defined medium. Stem Cell Res 3: 157–169.
15. Johansson BM, Wiles MV (1995) Evidence for involvement of activin A and bone morphogenetic protein 4 in mammalian mesoderm and hematopoietic development. Mol Cell Biol 15: 141–151.
16. Labastie MC, Cortes F, Romeo PH, Dulac C, Peault B (1998) Molecular identity of hematopoietic precursor cells emerging in the human embryo. Blood 92: 3624–3635.
17. Jones CM, Kuehn MR, Hogan BL, Smith JC, Wright CV (1995) Nodal-related signals induce axial mesoderm and dorsalize mesoderm during gastrulation. Development 121: 3651–3662.
18. Hart AH, Hartley L, Sourris K, Stadler ES, Li R, et al. (2002) Mixl1 is required for axial mesendoderm morphogenesis and patterning in the murine embryo. Development 129: 3597–3608.
19. Blum M, Gaunt SJ, Cho KW, Steinbeisser H, Blumberg B, et al. (1992) Gastrulation in the mouse: the role of the homeobox gene goosecoid. Cell 69: 1097–1106.
20. Wilkinson DG, Bhatt S, Herrmann BG (1990) Expression pattern of the mouse T gene and its role in mesoderm formation. Nature 343: 657–659.
21. Russ AP, Wattler S, Colledge WH, Aparicio SA, Carlton MB, et al. (2000) Eomesodermin is required for mouse trophoblast development and mesoderm formation. Nature 404: 95–99.
22. Chapman DL, Papaioannou VE (1998) Three neural tubes in mouse embryos with mutations in the T-box gene Tbx6. Nature 391: 695–697.
23. Saga Y, Hata N, Koseki H, Taketo MM (1997) Mesp2: a novel mouse gene expressed in the presegmented mesoderm and essential for segmentation initiation. Genes Dev 11: 1827–1839.
24. Williams BA, Ordahl CP (1994) Pax-3 expression in segmental mesoderm marks early stages in myogenic cell specification. Development 120: 785–796.
25. Ott MO, Bober E, Lyons G, Arnold H, Buckingham M (1991) Early expression of the myogenic regulatory gene, myf-5, in precursor cells of skeletal muscle in the mouse embryo. Development 111: 1097–1107.
26. Reshef R, Maroto M, Lassar AB (1998) Regulation of dorsal somitic cell fates: BMPs and Noggin control the timing and pattern of myogenic regulator expression. Genes Dev 12: 290–303.
27. Yamamoto H, Kishida S, Kishida M, Ikeda S, Takada S, et al. (1999) Phosphorylation of axin, a Wnt signal negative regulator, by glycogen synthase kinase-3beta regulates its stability. J Biol Chem 274: 10681–10684.
28. Nichols J, Zevnik B, Anastassiadis K, Niwa H, Klewe-Nebenius D, et al. (1998) Formation of pluripotent stem cells in the mammalian embryo depends on the POU transcription factor Oct4. Cell 95: 379–391.
29. Chambers I, Colby D, Robertson M, Nichols J, Lee S, et al. (2003) Functional expression cloning of Nanog, a pluripotency sustaining factor in embryonic stem cells. Cell 113: 643–655.
30. Mitsui K, Tokuzawa Y, Itoh H, Segawa K, Murakami M, et al. (2003) The homeoprotein Nanog is required for maintenance of pluripotency in mouse epiblast and ES cells. Cell 113: 631–642.
31. Kudoh H, Ikeda H, Kakitani M, Ueda A, Hayasaka M, et al. (2005) A new model mouse for Duchenne muscular dystrophy produced by 2.4 Mb deletion of dystrophin gene using Cre-loxP recombination system. Biochem Biophys Res Commun 328: 507–516.
32. Hoffman EP, Brown RH, Jr., Kunkel LM (1987) Dystrophin: the protein product of the Duchenne muscular dystrophy locus. Cell 51: 919–928.
33. Fukada S, Higuchi S, Segawa M, Koda K, Yamamoto Y, et al. (2004) Purification and cell-surface marker characterization of quiescent satellite cells from murine skeletal muscle by a novel monoclonal antibody. Exp Cell Res 296: 245–255.
34. Seale P, Sabourin LA, Girgis-Gabardo A, Mansouri A, Gruss P, et al. (2000) Pax7 is required for the specification of myogenic satellite cells. Cell 102: 777–786.
35. Avilion AA, Nicolis SK, Pevny LH, Perez L, Vivian N, et al. (2003) Multipotent cell lineages in early mouse development depend on SOX2 function. Genes Dev 17: 126–140.
36. Nostro MC, Cheng X, Keller GM, Gadue P (2008) Wnt, activin, and BMP signaling regulate distinct stages in the developmental pathway from embryonic stem cells to blood. Cell Stem Cell 2: 60–71.
37. Okita K, Ichisaka T, Yamanaka S (2007) Generation of germline-competent induced pluripotent stem cells. Nature 448: 313–317.
38. Ogawa K, Saito A, Matsui H, Suzuki H, Ohtsuka S, et al. (2007) Activin-Nodal signaling is involved in propagation of mouse embryonic stem cells. J Cell Sci 120: 55–65.
39. Tada S, Era T, Furusawa C, Sakurai H, Nishikawa S, et al. (2005) Characterization of mesendoderm: a diverging point of the definitive endoderm and mesoderm in embryonic stem cell differentiation culture. Development 132: 4363–4374.
40. Kattman SJ, Witty AD, Gagliardi M, Dubois NC, Niapour M, et al. (2011) Stage-specific optimization of activin/nodal and BMP signaling promotes cardiac differentiation of mouse and human pluripotent stem cell lines. Cell Stem Cell 8: 228–240.
41. Wang Y, Umeda K, Nakayama N (2010) Collaboration between WNT and BMP signaling promotes hemoangiogenic cell development from human fibroblast-derived iPS cells. Stem Cell Res 4: 223–231.
42. Laping NJ, Grygielko E, Mathur A, Butter S, Bomberger J, et al. (2002) Inhibition of transforming growth factor (TGF)-beta1-induced extracellular matrix with a novel inhibitor of the TGF-beta type I receptor kinase activity: SB-431542. Mol Pharmacol 62: 58–64.
43. Okita K, Nakagawa M, Hyenjong H, Ichisaka T, Yamanaka S (2008) Generation of mouse induced pluripotent stem cells without viral vectors. Science 322: 949–953.
44. Nakagawa M, Koyanagi M, Tanabe K, Takahashi K, Ichisaka T, et al. (2008) Generation of induced pluripotent stem cells without Myc from mouse and human fibroblasts. Nat Biotechnol 26: 101–106.
45. Nishikawa SI, Nishikawa S, Hirashima M, Matsuyoshi N, Kodama H (1998) Progressive lineage analysis by cell sorting and culture identifies FLK1+VE-cadherin+ cells at a diverging point of endothelial and hemopoietic lineages. Development 125: 1747–1757.
46. Muraglia A, Corsi A, Riminucci M, Mastrogiacomo M, Cancedda R, et al. (2003) Formation of a chondro-osseous rudiment in micromass cultures of human bone-marrow stromal cells. J Cell Sci 116: 2949–2955.
47. Sakurai H, Okawa Y, Inami Y, Nishio N, Isobe KI (2008) Paraxial Mesodermal Progenitors Derived from Mouse Embryonic Stem Cells Contribute Muscle Regeneration via Differentiation into Muscle Satellite Cells. Stem Cells.

OPEN ACCESS Freely available online

PLOS | ONE

VCP Is an Integral Component of a Novel Feedback Mechanism that Controls Intracellular Localization of Catalase and H_2O_2 Levels

Katsuhiro Murakami[1], Yuzuru Ichinohe[1], Masaaki Koike[1], Norio Sasaoka[1], Shun-ichiro Iemura[2], Tohru Natsume[2], Akira Kakizuka[1]*

1 Laboratory of Functional Biology, Kyoto University Graduate School of Biostudies, Sakyo-ku, Kyoto, Japan, **2** National Institutes of Advanced Industrial Science and Technology, Biological Information Research Center (JBIRC), Kohtoh-ku, Tokyo, Japan

Abstract

Catalase is a key antioxidant enzyme that catalyzes the decomposition of hydrogen peroxide (H_2O_2) to water and oxygen, and it appears to shuttle between the cytoplasm and peroxisome via unknown mechanisms. Valosin-containing protein (VCP) belongs to the AAA class of ATPases and is involved in diverse cellular functions, e.g. cell cycle and protein degradation, etc. Here we show that VCP and PEX19, a protein essential for peroxisome biogenesis, interact with each other. Knockdown of either VCP or PEX19 resulted in a predominantly cytoplasmic redistribution of catalase, and loss of VCP ATPase activity also increased its cytoplasmic redistribution. Moreover, VCP knockdown decreased intracellular ROS levels in normal and H_2O_2-treated cells, and an oxidation-resistant VCP impaired the ROS-induced cytoplasmic redistribution of catalase. These observations reveal a novel feedback mechanism, in which VCP can sense H_2O_2 levels, and regulates them by controlling the localization of catalase.

Citation: Murakami K, Ichinohe Y, Koike M, Sasaoka N, Iemura S-i, et al. (2013) VCP Is an Integral Component of a Novel Feedback Mechanism that Controls Intracellular Localization of Catalase and H_2O_2 Levels. PLoS ONE 8(2): e56012. doi:10.1371/journal.pone.0056012

Editor: Junji Yodoi, Institute for Virus Research, Laboratory of Infection and Prevention, Japan

Received October 2, 2012; **Accepted** January 4, 2013; **Published** February 14, 2013

Funding: This work was supported in part by research grants from Solution Oriented Research for Science and Technology (SORST) of Japan Science and Technology Agency (JST), the Ministry of Education, Culture, Sports, Science, and Technology of Japan, and the Ministry of Health, Labour, and Welfare of Japan. The funders had no role in study design, data collection and analysis, decision to publish, or preparation of the manuscript.

Competing Interests: The authors have declared that no competing interests exist.

* E-mail: kakizuka@lif.kyoto-u.ac.jp

Introduction

Reactive oxygen species (ROS), e.g. superoxide radicals, hydrogen peroxide, etc., are natural byproducts of the aerobic metabolism of foods, and they have been shown to play important roles in several physiological functions, e.g. transcriptional regulation, mitogen signaling, integrin signaling, Wnt signaling, etc. (see refs in [1–3]). On the other hand, ROS are also produced by UV and X-ray exposure or inflamation, and excess ROS can damage cellular functions by oxidizing proteins, lipids, and DNA, leading to cell aging as well as cancer (see refs in [4]). Among ROS, the superoxide radical is enzymatically converted by superoxide dismutases (SODs) to hydrogen peroxide (H_2O_2), which, in turn, is converted by catalase or peroxidases to H_2O and O_2. Mammalian cells typically possess three SODs, several peroxidases, and one catalase. Among these ROS-scavenging enzymes, only catalase resides in peroxisomes. In certain conditions, such as aging, catalase also resides in the cytoplasm [5], which is believed to be due to its weak peroxisome-targeting signal (PTS). Two types of PTS, PTS1 and PTS2, are known [6]. Typically, PTS1 consists of three sequential amino acids, SKL, and it is present in peroxisome-localized proteins such as peroxisomal Acyl-CoA thioesterase, PTE1. Catalase has a unique PTS1, consisting of four sequential amino acids, KANL. Both PTS1s are recognized by PEX5 (Peroxisome biogenesis factor 5); however, PEX5 binds to SKL more strongly than to KANL [7], and thus it is believed that PEX5 can transfer SKL-containing proteins more effectively than catalase to peroxisomes. In aged cells, cellular levels of ROS increase, and it is thought that such ROS may weaken PEX5 functions, with transport of catalase to peroxisomes being preferentially compromised, as opposed to transport of SKL-possessing proteins [8]. However, no clear evidence has been provided supporting this speculation.

VCP belongs to the AAA class of ATPases and has been shown to function in many cellular events, including ERAD (endoplasmic reticulum-associated degradation), cell cycle control, membrane fusion, maintenance of Golgi apparatus, protein aggregate formation and clearance, etc. (see refs in [9]). VCP has also been shown to play important roles in several human neurodegenerative disorders [10–12]. We have shown that VCP is modified post-translationally at 60 amino acids, at least, including 18 serines, 14 threonines, 6 tyrosines, and 22 lysines [13]. To investigate the role of post-transcriptional modifications of VCP, we created several modification-mimic forms of VCP, and characterized them [12–14]. These analyses have revealed novel VCP functions and have led us to speculate that VCP may have unidentified functions. In this study, we report a novel VCP function in regulation of intracellular H_2O_2 levels via the control of catalase localization.

Materials and Methods

Antibodies

The following antibodies were purchased: anti-actin (Chemicon), anti-catalase (Calbiochem), anti-PTE1 (ACOT8) (Santa Cruz), anti-FLAG M2 (Sigma), anti-PMP70 (Zymed), anti-HA (Santa Cruz), and anti-PEX19 (BD PharMingen). The affinity-purified rabbit polyclonal anti-VCP antibody was described previously [15].

Plasmids and siRNAs

The cDNAs for PEX5, PEX19, catalase, and PTS2 signal sequences of ACAA1 (acetyl-CoA acyltransferase 1) were amplified by RT–PCR from total RNA isolated from HeLa cells, and their sequences were confirmed. The VCP cDNAs (wtVCP, VCP[K251A], VCP[K524A] [16]) or PEX5 cDNA was subcloned into pmCherry vector (Clontech). The PEX19 cDNA was subcloned into pCMV-HA vector (Clontech).

The targeting sequences of siRNAs for VCP and PEX5 mRNAs were as follows:

VCP(nc), 5′-CGGGAGAGGCGCGCGCCAT-3′;
VCP(286), 5′-GGTTAATTGTTGATGAAGCCATCAA-3′;
PEX5(192), 5′-CAAGCCTTTGGGAGTAGCTTCTGAA-3′;
PEX5(955), 5′-GACCTTACGTCAGCTACCTATGATA-3′.
Control, 5′-CGGACGCGTCAGGAGCCGGTT-3′.

The siRNAs for PEX19 were purchased from Invitrogen (Stealth Select RNAi, HSS108913 and HSS108914, respectively).

Cell Culture and Cell Lines

HeLa cells and HEK293A cells were grown at 37°C in Dulbecco's modified Eagle's medium supplemented with 10% fetal bovine serum. HeLa cell lines stably expressing organelle-targeted GFPs were created by transfection of organelle-targeted GFP expression vectors, and selected in the presence of 2.5 μg/ml of puromycin (Invivogen). The HEK293A cell line stably expressing GFP-catalase, was also created by similar methods.

Transfection and Immunostaining

Plasmid transfection was carried out using Lipofectamine plus (Invitrogen), and siRNA transfection was carried out using Oligofectamine (Invitrogen) according to the manufacturer's protocol. In co-transfection experiments, cells were transfected with siRNA and plasmid using Lipofectamine 2000 (Invitrogen).

Cells were fixed with 4% formaldehyde for 10 min at room temperature. Fixed cells were permeabilized with 0.5% Triton X-100 in PBS for 10 min at room temperature and blocked with blocking buffer (0.1% bovine serum albumin and 0.1% skim milk in PBS) for 1 h. Cells were then incubated 1 h at room temperature with primary antibodies. Subsequently, cells were treated with Alexa Fluor 488-conjugated secondary antibodies (Invitrogen). To detect PMP70, fixed cells were permeabilized with 25 μg/ml digitonin in PBS for 5 min at room temperature, and cells were processed for immunostaining as describe above.

Subcellular Fractionation and Immunoprecipitation

Cells were fractionated into cytosol, membrane/organelle, and nucleus, using a Subcellular Proteome extraction kit (Calbiochem), according to the manufacturer's protocol. Immunoprecipitation assays were performed as described previously [16]. Briefly, samples were lysed on ice and debris was removed by centrifugation for 30 min at 15,000×g at 4°C. The supernatant was mixed with an anti-HA or anti-FLAG antibody and rotated at 4°C overnight after addition of protein G-Sepharose beads (Amersham Biosciences). After washing of beads, bound proteins were analyzed by Western blot.

Intracellular ROS Detection

Cells were washed twice with HBSS and incubated with 5 μM CM-H_2DCFDA, a ROS-detection reagent (Invitrogen), in HBSS at 37°C for 30 min. Subsequently, cells were washed twice with HBSS and incubated with growth medium at 37°C for 30 min with or without H_2O_2. Then cells were analyzed by FACScan flow cytometer (BD Biosciences) or LSM510 confocal microscopy (Carl Zeiss).

Statistical Analysis

Each experiment was conducted at least three times with consistent results. The gel or blot representative of each experiment is presented in this study. The statistical significance was analyzed using Student's *t* test.

Results

Involvement of VCP in Intracellular Localization of Catalase

In order to visualize organelle in live cells, we generated several HeLa cell sublines in which GFP was expressed as a fusion protein with a peroxisomal (PTS1 or PTS2)-, nuclear (NLS)-, ER (KDEL)-, or mitochondrial (mito)-targeting signal. Among these, we observed clear mislocalization of GFP-PTS1 (namely, GFP-SKL and GFP-KANL) into the cytoplasm when the cells were treated with VCP siRNAs but not a control siRNA. VCP siRNAs perturbed GFP-KANL localization much more severely than GFP-SKL localization (**Fig. 1A and B**). By contrast, VCP siRNAs did not induce clear mislocalization of PTS2-GFP, mito-GFP, GFP-ER, or GFP-NLS (Fig. S1). We observed similar mislocalization of GFP-KANL by expressing ATPase-negative or dominant-negative VCP mutants, e.g. VCP[K251A] and VCP[K524A] [16] (Fig. S2). In addition, treating cells with DBeQ, a VCP inhibitor [17], also induced cytoplasmic localization of GFP-catalase (**Fig. 1C**). These results suggest that the ATPase activity of VCP is necessary for proper localization of catalase.

We then examined the effects of VCP knockdown on intracellular localization of endogenous PTE1 or catalase. In more than 50% of cells treated with VCP siRNAs, endogenous catalase was diffusely observed in the cytoplasm. In contrast, PTE1 localization was not apparently affected by VCP knockdown (**Fig. 1D**). These results were confirmed by cell fractionation experiments. VCP siRNA treatments increased the amounts of catalase but not PTE1 in the cytoplasmic fraction (**Fig. 1E**). Mislocalization of catalase as well as GFP-KANL decreased in cells treated with VCP siRNA together with cycloheximide (Fig. S3), supporting the idea that newly synthesized catalase is transported into peroxisomes with the help of VCP.

Interaction between VCP and PEX19

In order to obtain insights for molecular mechanisms underlying VCP-mediated regulation of catalase localization, we searched for VCP-interacting proteins using an immunoprecipitation method followed by a very sensitive MS/MS analysis [18], and identified PEX19 as a potential VCP-interacting protein. Indeed, we could observe a physical association between VCP and PEX19 via immunoprecipitation and western blotting (**Fig. 2**). This interaction appeared very weak, suggesting the possibility that yet-unknown VCP modification may enhance this interaction. This possibility remained to be clarified.

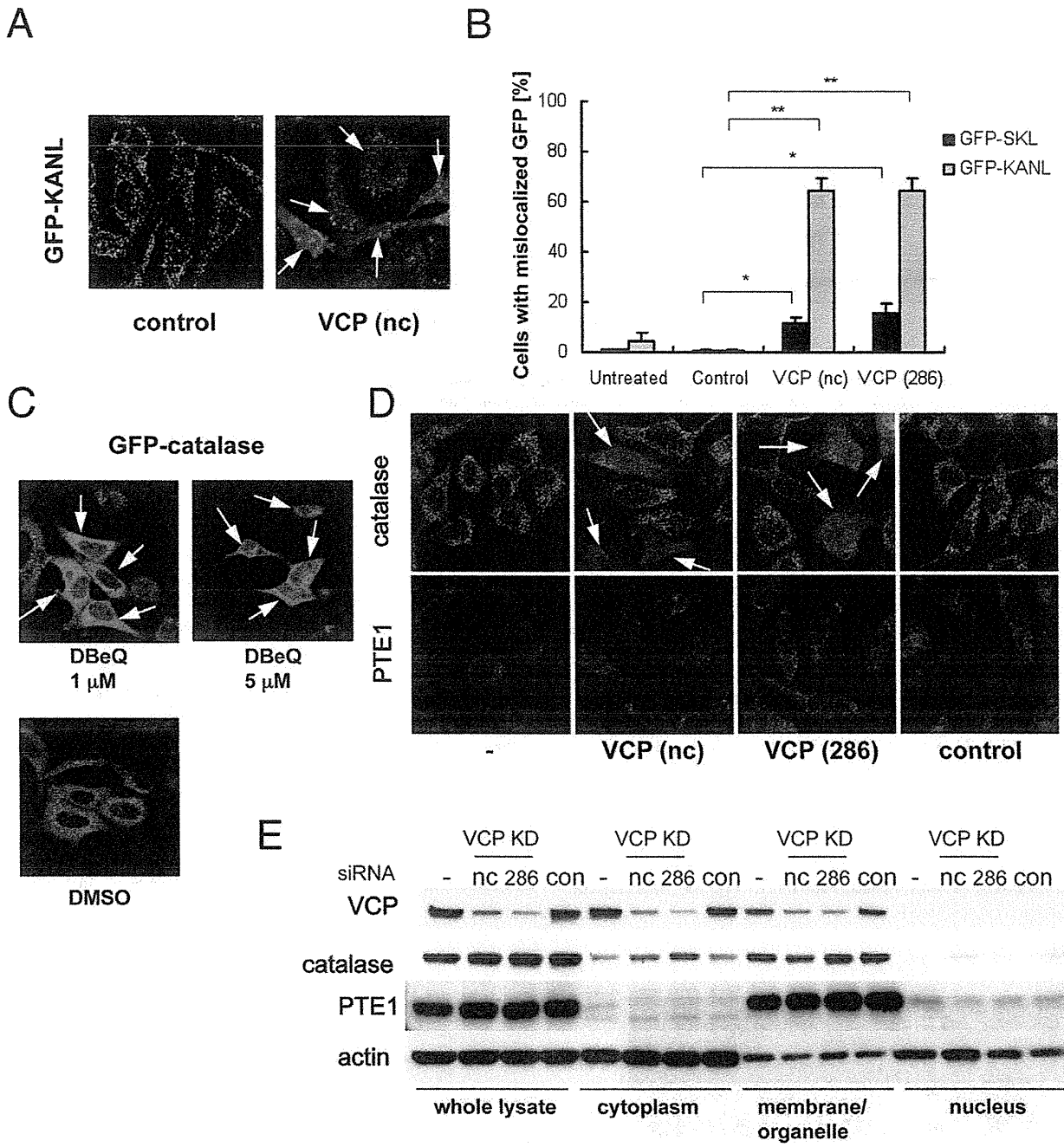

Figure 1. VCP siRNAs induce cytoplasmic localization of catalase. (A) Cytochemical analysis of intracellular localization of GFP-KANL. HeLa cells continuously expressing GFP-KANL were treated with control siRNA (control) or VCP siRNAs (nc and 286). Seventy-two hours later, GFP images were analyzed by confocal microscopy. Arrows indicate cells with cytoplasmic localization of GFP-KANL. (B) Quantification of cytochemical analysis on GFP-KANL in (A) and on GFP-SKL. More than 200 cells were examined in each sample, and the fraction (%) of cells with diffuse GFP signals in the cytoplasm were scored. $^{**}p<0.01$, $^{*}p<0.05$. (C) Fluorescence microscopy analysis of intracellular localization of GFP-catalase. HEK293A cells continuously expressing GFP-catalase were treated with 1 μM or 5 μM DBeQ, a VCP inhibitor [17], or DMSO for 24 hours, and then GFP signals were detected. Arrows indicate cells with cytoplasmic localization of GFP-catalase. (D) Immunocytochemical analysis of intracellular localization of catalase and PTE1. HeLa cells were treated without (−) or with control siRNA (control), or VCP siRNAs (nc and 286). Seventy-two hours later, catalase and PTE1 were detected with anti-catalase and anti-PTE1 antibodies, respectively. Arrows indicate cells with cytoplasmic localization of catalase. (E) Western blot analyses of protein levels of VCP, catalase, and PTE1 in different cell compartments. HeLa cells were treated without (−) or with control siRNA (control) or VCP siRNAs (nc and 286). Seventy-two hours later, cells were fractionated as described in Methods. Fractionated samples equivalent to 7.5 μg total protein of whole cell lysates were separated by SDS-PAGE and analyzed by western blotting using specific antibodies. Actin served as a loading control.

doi:10.1371/journal.pone.0056012.g001

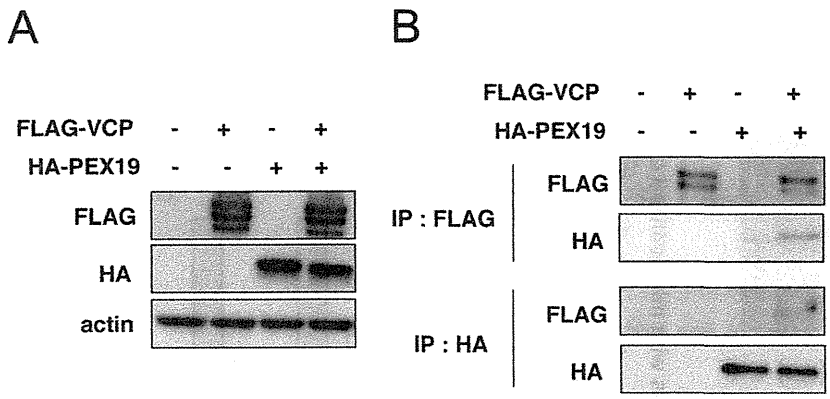

Figure 2. Immunoprecipitation assays to detect physical interactions between VCP and PEX19. (A) HEK293A cells were transfected with expression vectors for FLAG-VCP and HA-PEX19. Twenty-four hours later, cells were harvested and the cell lysates were analyzed by western blots with antibodies indicated in the panels. Actin served as a loading control. (B) The immunoprecipitation was performed on the cell lysates in (A) with an anti-FLAG or anti-HA antibody. The precipitates were analyzed by western blots with antibodies indicated in the panels. See details in **Materials and methods.**
doi:10.1371/journal.pone.0056012.g002

Involvement of PEX19 in Intracellular Localization of Catalase

Given that VCP could potentially make a complex with PEX19 and that VCP knockdown apparently affected the transport of catalase into peroxisomes, PEX19 knockdown could also affect the intracellular localization of catalase. Indeed, PEX19 knockdowns produced virtually identical distributions of intracellular catalase as were observed in VCP knockdowns (**Fig. 3A and B**). Moreover, in PEX19 knockdown cells, PTE1 localization was not apparently affected (**Fig. 3A and B**). PEX19 is reportedly involved in the transport of membrane proteins, such as PMP70 (peroxisome membrane protein 70), to peroxisomes. However, we could not detect any clear mislocalization of endogenous PMP70 in VCP-depleted HeLa cells (Fig. S4).

Consistent with previous reports, PEX5 knockdown induced mislocalization of both catalase and PTE1 (Fig. S5). It is notable that over-expression of PEX5 and VCP could not rectify the mislocalization of GFP-KANL in VCP and PEX5 knockdown cells, respectively (Fig. S6). These results indicate that VCP/PEX19 complexes are required for PEX5 to transport catalase, but not other typical PTS1- or PTS2-possessing proteins, to peroxisomes.

VCP Activity, Catalase Localization, and ROS Levels

We next examined the possibility that VCP-depleted cells have a greater capacity to scavenge H_2O_2 as compared with non-treated cells, due to the presence of catalase in the cytoplasm. This was indeed the case. Basal ROS levels were reduced in cells treated with VCP siRNAs compared to those treated with control siRNAs (**Fig. 4A**). Reduction of ROS levels was more pronounced when cells were treated with H_2O_2 (**Fig. 4A and B**). We have previously shown that the ATPase activity of VCP was inactivated

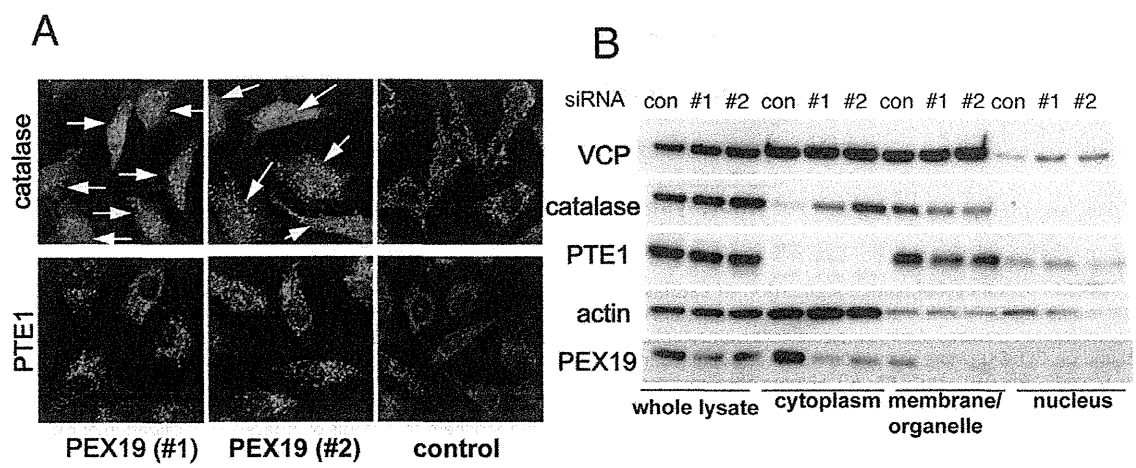

Figure 3. PEX19 siRNAs also induce cytoplasmic localization of catalase. (A) Immunocytochemical analysis of intracellular localization of catalase and PTE1. HeLa cells were treated with control siRNA (control) or PEX19 siRNAs (#1; HSS108913 and #2; HSS108914). Seventy-two hours later, catalase and PTE1 were detected as in (Fig. 1D). Arrows indicate cells with cytoplasmic localization of catalase. (B) Western blot analyses of protein levels of VCP, catalase, PTE1, and PEX19 in different cell compartments. HeLa cells were treated with control siRNA (control) or PEX19 siRNAs (#1; HSS108913 and #2; HSS108914). Seventy-two hours later, cells were analyzed as in (Fig. 1E).
doi:10.1371/journal.pone.0056012.g003

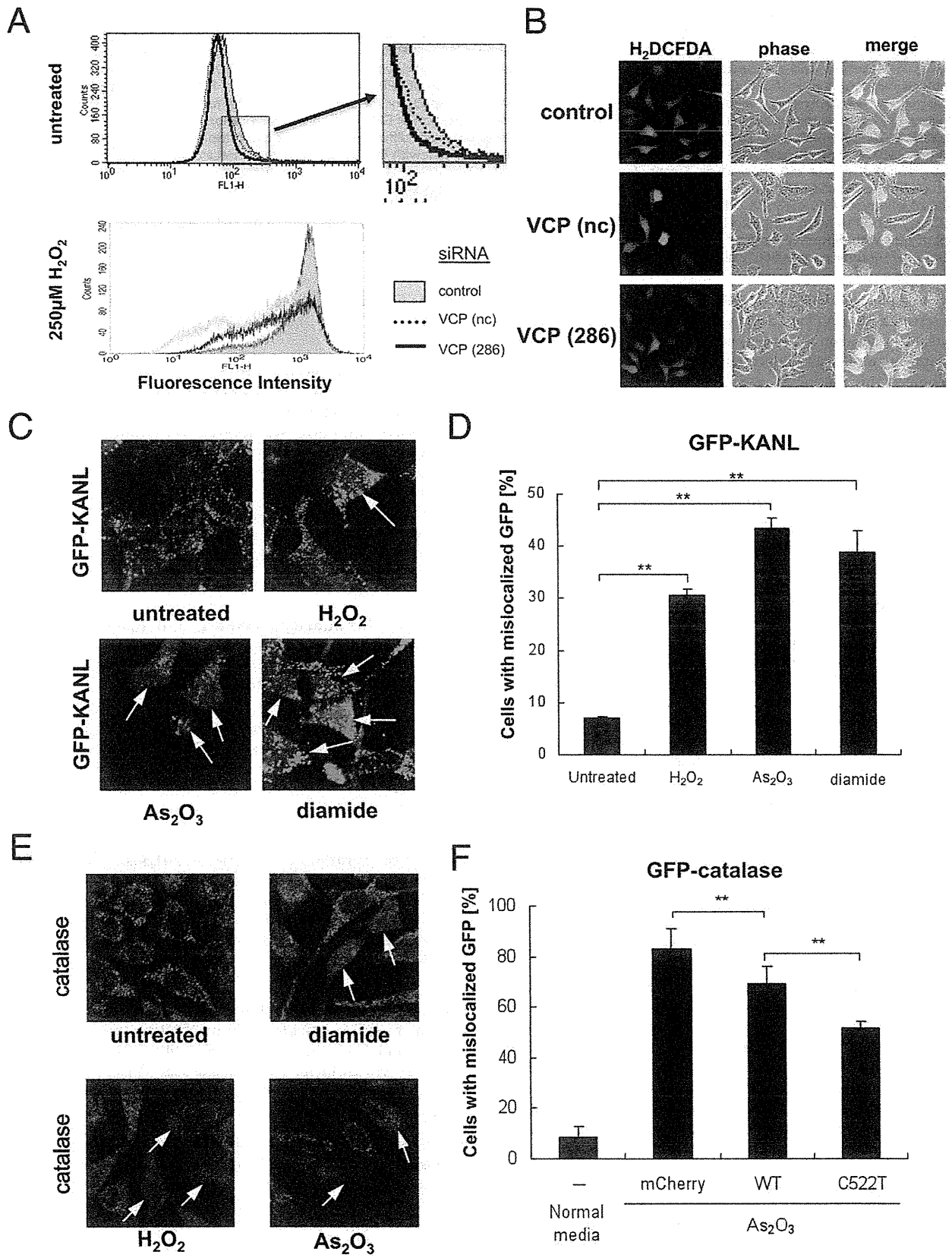
A
untreated
Counts
FL1-H
250μM H_2O_2
siRNA
control
VCP (nc)
VCP (286)
Fluorescence Intensity
B
H_2DCFDA
phase
merge
control
VCP (nc)
VCP (286)
C
GFP-KANL
untreated
H_2O_2
As_2O_3
diamide
D
GFP-KANL
Cells with mislocalized GFP [%]
Untreated
H_2O_2
As_2O_3
diamide
E
catalase
untreated
diamide
H_2O_2
As_2O_3
F
GFP-catalase
Cells with mislocalized GFP [%]
Normal media
mCherry
WT
C522T
As_2O_3

Figure 4. ROS levels and intracellular localization of GFP-KANL and catalase in cells with VCP depletion or overexpression. (A) ROS levels in cells with VCP depletion. HeLa cells were treated with control (control) or VCP (nc and 286) siRNAs. Seventy-two hours later, 5 μM H_2DCFDA was added to the media for 30 min. Then, cells were treated with or without 250 μM H_2O_2 at 37°C for additional 30 min, and analyzed by FACS (see details in **Materials and methods**). (B) Cytochemical analysis of HeLa cells treated with 250 μM H_2O_2. H_2DCFDA fluorescence was analyzed by confocal microscopy as in (A). (C) Cytochemical analysis of intracellular localization of GFP-KANL after treatment of ROS-producing agents. HEK293A cells continuously expressing GFP-KANL were treated with 250 μM H_2O_2, 20 nM As_2O_3, or 250 μM diamide. Twenty-four hours later, GFP images were analyzed by confocal microscopy. Arrows indicate cells with cytoplasmic localization of GFP-KANL. (D) Quantification of cytochemical analysis in (C). More than 200 cells were examined in each sample, and the fraction (%) of cells with diffuse GFP signals in the cytoplasm were scored. $^{**}p<0.01$. (E) Immunocytochemical analysis of intracellular localization of catalase after treatment with ROS-producing agents. HeLa cells were treated with 500 μM H_2O_2, 20 nM As_2O_3, or 250 μM diamide. Twenty-four hours later, catalase was detected with an anti-catalase antibody. Arrows indicate cells with cytoplasmic localization of catalase. (F) Overexpression of VCP[C522T] weakened cytoplasmic localization of catalase by ROS more significantly than that of wild-type VCP. HEK293A cells continuously expressing GFP-catalase were transfected with VCP[C522T]-mCherry (C522T) or wild-type VCP-mCherry (wtVCP), and treated with 20 nM As_2O_3 for 24 hours. More than 200 mCherry-positive cells were examined in each sample, and the fraction (%) of cells with diffuse GFP signals in the cytoplasm were scored. $^{**}p<0.01$.
doi:10.1371/journal.pone.0056012.g004

by oxidation of Cys522 by ROS, such as H_2O_2 [14]. The observation that ATPase activity of VCP is necessary for proper catalase localization to peroxisomes raised the possibility that ROS treatments would also induce redistribution of catalase. We next examined this possibility, and confirmed that all tested ROS-inducing agents (such as H_2O_2, As_2O_3, and diamide) induced cytoplasmic localization of GFP-KANL as well as catalase (**Fig. 4C–E**). We then examined whether VCP[C522T], a VCP mutant with the ROS-sensitive cysteine to threonine substitution [14], had protective effects on redistribution of catalase in cells treated with ROS. Indeed, overexpression of VCP[C522T] significantly inhibited cytoplasmic localization of catalase in cells treated with As_2O_3, compared to overexpressed wild-type VCP (**Fig. 4F**).

Discussion

The results presented in this study, taken together, point to the existence of a novel feedback mechanism: when H_2O_2 levels increase, VCP ATPase is inactivated by Cys522 oxidation, which in turn keeps catalase in the cytoplasm, leading to reduced H_2O_2 levels. After H_2O_2 levels are reduced, glutathione as well as thioredoxine levels would recover, which would then restore VCP ATPase activity, leading to catalase transport into peroxisomes. This VCP-mediated system has the great merit of specifically changing the localization of catalase without affecting the localization of other peroxisome proteins.

In *S. cerevisiae*, Cys522 is not conserved in Cdc48p, a VCP homologue [14]. In what appears to be an evolutionary alternative design, *S. cerevisiae* possesses two catalases, one of which resides in peroxisomes and the other in the cytoplasm [19,20]. *C. elegans* also possesses two catalases, one in peroxisomes and the other in the cytoplasm [21]. These lines of evidence strongly indicate that for living organisms catalase is needed in both peroxisomes and the cytoplasm. In mammals, a certain level of ROS, namely H_2O_2, is utilized in several physiological conditions, and, therefore the continuous presence of catalase in the cytoplasm might not be favorable. On the other hand, when mammalian cells meet conditions with a large amount of H_2O_2 in the cytoplasm, catalase would more effectively degrade and reduce H_2O_2 by accumulating in the cytoplasm. Thus, mammals have developed an integrated system to utilize one catalase rather than to have two differently localized catalases.

Supporting Information

Figure S1 Fluorescence microscopy analysis of intracellular localization of PTS2-GFP, mito-GFP, GFP-ER, and GFP-NLS. (A) Schematic drawings of GFP-fused proteins. (B) HeLa cells were treated with control siRNA (control) or VCP siRNAs (nc and 286). Seventy-two hours later, GFP signals were detected.
(TIFF)

Figure S2 Fluorescence microscopy analysis of intracellular localization of GFP-KANL in the presence of ATPase activity-defective mutant VCPs. (A) HEK293A cells continuously expressing GFP-KANL were transfected with an expression vectors for mCherry or VCP (wtVCP, VCP[K251A] [15], or VCP[K524A] [15])-mCherry. Forty-eight hours later, GFP signals were detected. (B) Quantification of fluorescence microscopy of GFP-KANL in (A). More than 200 mCherry-positive cells were examined in each sample, and the fraction (%) of cells with diffuse GFP signals in the cytoplasm were scored. $^{**}p<0.01$, $^{*}p<0.05$.
(TIFF)

Figure S3 Immunocytochemical and fluorescence microscopy analyses of intracellular localization of catalase and GFP-KANL. (A) HeLa cells were treated with control siRNA (control) or VCP siRNA (286) for 72 hours, and treated with or without cyclohexamide (CHX) (5 μg/ml) for additional 24 hours. Then catalase was detected with anti-catalase antibody. (B) HeLa cells continuously expressing GFP-KANL were treated with VCP siRNA (286). Cells were treated with or without 5 μg/ml of CHX from 48 (24 h) or 24 (48 h) to 72 hours after siRNA treatment. Then, GFP signals were detected.
(TIFF)

Figure S4 Immunocytochemical analysis of intracellular localization of PMP70. HeLa cells were treated without (−) or with control siRNA (control), or VCP siRNAs (nc and 286). Seventy-two hours later, PMP70 was detected with an anti-PMP70 antibody. Note that VCP protein levels decreased by VCP siRNA treatments, as shown in Fig. 1E
(TIFF)

Figure S5 Immunocytochemical analysis of intracellular localization of catalase and PTE1. HeLa cells were treated with control siRNA (control) or PEX5 siRNAs (192 and 955). Seventy-two hours later, catalase and PTE1 were detected with anti-catalase and anti-PTE1 antibodies, respectively.
(TIFF)

Figure S6 Fluorescence microscopy analysis of intracellular localization of GFP-KANL. (A) HeLa cells continuously expressing GFP-KANL were treated with control siRNA (control), VCP siRNA (nc), or PEX5 siRNA (192) for 48 hours, and then transfected with an expression vector for mCherry, VCP-mCherry, or mCherry-PEX5. Twenty-four hours later, GFP signals (green) and mCherry signals (red) were examined. (B) Quantification of fluorescence microscopy of GFP-KANL in (A).

More than 120 mCherry-positive cells were examined in each sample, and the fraction (%) of cells with diffuse GFP signals in the cytoplasm were scored. n.s., not significant.
(TIFF)

Acknowledgments

We thank Professor James A. Hejna (Kyoto University) for critical reading of the manuscript.

References

1. Vurusaner B, Poli G, Basaga H (2012) Tumor suppressor genes and ROS: complex networks of interactions. Free Radic Biol Med 52: 7–18.
2. Funato Y, Miki H (2010) Redox regulation of Wnt signalling via nucleoredoxin. Free Radic Res 44: 379–388.
3. Hu CT, Wu JR, Cheng CC, Wang S, Wang HT, et al. (2011) Reactive oxygen species-mediated PKC and integrin signaling promotes tumor progression of human hepatoma HepG2. Clin Exp Metastasis 28: 851–863.
4. Valko M, Leibfritz D, Moncol J, Cronin MT, Mazur M, et al. (2007) Free radicals and antioxidants in normal physiological functions and human disease. Int J Biochem Cell Biol 39: 44–84.
5. Legakis JE, Koepke JI, Jedeszko C, Barlaskar F, Terlecky LJ, et al. (2002) Peroxisome senescence in human fibroblasts. Mol Biol Cell 13: 4243–4255.
6. Heiland I, Erdmann R (2005) Biogenesis of peroxisomes. Topogenesis of the peroxisomal membrane and matrix proteins. FEBS J 272: 2362–2372.
7. Maynard EL, Gatto GJ Jr, Berg JM (2004) Pex5p binding affinities for canonical and noncanonical PTS1 peptides. Proteins 55: 856–861.
8. Terlecky SR, Koepke JI, Walton PA (2006) Peroxisomes and aging. Biochim Biophys Acta 1763: 1749–1754.
9. Manno A, Noguchi M, Fukushi J, Motohashi Y, Kakizuka A (2010) Enhanced ATPase activities as a primary defect of mutant valosin-containing proteins that cause inclusion body myopathy associated with Paget disease of bone and frontotemporal dementia. Genes Cells 15: 911–922.
10. Kakizuka A (2008) Roles of VCP in human neurodegenerative disorders. Biochem Soc Trans 36: 105–108.
11. Johnson JO, Mandrioli J, Benatar M, Abramzon Y, Van Deerlin VM, et al. (2010) Exome sequencing reveals VCP mutations as a cause of familial ALS. Neuron 68: 857–864.
12. Koike M, Fukushi J, Ichinohe Y, Higashimae N, Fujishiro M, et al. (2010) Valosin-containing protein (VCP) in novel feedback machinery between abnormal protein accumulation and transcriptional suppression. J Biol Chem 285: 21736–21749.
13. Mori-Konya C, Kato N, Maeda R, Yasuda K, Higashimae N, et al. (2009) p97/valosin-containing protein (VCP) is highly modulated by phosphorylation and acetylation. Genes Cells 14: 483–497.
14. Noguchi M, Takata T, Kimura Y, Manno A, Murakami K, et al. (2005) ATPase activity of p97/valosin-containing protein is regulated by oxidative modification of the evolutionally conserved cysteine 522 residue in Walker A motif. J Biol Chem 280: 41332–41341.
15. Hirabayashi M, Inoue K, Tanaka K, Nakadate K, Ohsawa Y, et al. (2001) VCP/p97 in abnormal protein aggregates, cytoplasmic vacuoles, and cell death, phenotypes relevant to neurodegeneration. Cell Death Differ 8: 977–984.
16. Kobayashi T, Tanaka K, Inoue K, Kakizuka A (2002) Functional ATPase activity of p97/valosin-containing protein (VCP) is required for the quality control of endoplasmic reticulum in neuronally differentiated mammalian PC12 cells. J Biol Chem 277: 47358–47365.
17. Chou TF, Brown SJ, Minond D, Nordin BE, Li K, et al. (2011) Reversible inhibitor of p97, DBeQ, impairs both ubiquitin-dependent and autophagic protein clearance pathways. Proc Natl Acad Sci U S A 108: 4834–4839.
18. Natsume T, Yamauchi Y, Nakayama H, Shinkawa T, Yanagida M, et al. (2002) A direct nanoflow liquid chromatography-tandem mass spectrometry system for interaction proteomics. Anal Chem 74: 4725–4733.
19. Cohen G, Rapatz W, Ruis H (1988) Sequence of the Saccharomyces cerevisiae CTA1 gene and amino acid sequence of catalase A derived from it. Eur J Biochem 176: 159–163.
20. Hartig A, Ruis H (1986) Nucleotide sequence of the Saccharomyces cerevisiae CTT1 gene and deduced amino-acid sequence of yeast catalase T. Eur J Biochem 160: 487–490.
21. Togo SH, Maebuchi M, Yokota S, Bun-Ya M, Kawahara A, et al. (2000) Immunological detection of alkaline-diaminobenzidine-negativeperoxisomes of the nematode Caenorhabditis elegans purification and unique pH optima of peroxisomal catalase. Eur J Biochem 267: 1307–1312.

Author Contributions

Conceived and designed the experiments: KM AK. Performed the experiments: KM YI MK NS S-II. Analyzed the data: KM TN AK. Contributed reagents/materials/analysis tools: NS. Wrote the paper: KM AK.

Long-term oral administration of Hop flower extracts mitigates Alzheimer phenotypes in mice.

Norio Sasaoka,[1] Megumi Sakamoto,[1] Shoko Kanemori,[1] Chihiro Tsukano,[2] Yoshiji Takemoto,[2] and Akira Kakizuka[1]

[1]Laboratory of Functional Biology, Kyoto University Graduate School of Biostudies, Sakyo-ku, Kyoto, Japan.

[2]Department of Organic Chemistry, Kyoto University Graduate School of Pharmaceutical Science, Sakyo-ku, Kyoto, Japan

Key words: Hop flower extract; Alzheimer disease; prophylactics; γ-secretase inhibitor

Correspondence

Akira Kakizuka, Laboratory of Functional Biology, Kyoto University Graduate School of Biostudies, Kyoto 606-8501, Japan,

FAX: +81-75-753-7676

Tel: +81-75-753-7675

E-mail: kakizuka@lif.kyoto-u.ac.jp

Abstract

Coincident with the expanding population of aged people, the incidence of Alzheimer disease (AD) is rapidly increasing in most advanced countries. At present, no effective prophylactics are available. Among several pathological mechanisms proposed for AD, the "amyloid hypothesis" has been most widely accepted, in which accumulation or deposition of Aβ is considered to be the initial event. Thus, prevention of Aβ production would be an ideal strategy for the treatment or prevention of AD. Aβ is produced via the proteolytic cleavage of its precursor protein, APP (amyloid precursor protein), by two different enzymes, β and γ-secretases. Indeed, inhibitors against either or both enzymes have been developed and tested for clinical efficacy. Based on the "amyloid hypothesis", we developed a luciferase-based screening method to monitor γ-secretase activity, screened more than 1,600 plant extracts, most of which have long been used in Chinese medicine, and observed that Hop extracts significantly inhibit Aβ production in cultured cells. A major component of the inhibitory activity was purified, and its chemical identity was determined by NMR to be Garcinielliptone HC. *In vivo*, oral administration of Hop extracts to AD model mice decreased Aβ depositions in the cerebral cortex of the parietal lobe, hippocampus, and artery walls (amyloid angiopathy) in the brains. In a Morris water maze test, AD model mice that had daily consumed Hop extracts in their drinking water showed significant mitigation of memory impairment at ages of 9 and 12 months. Moreover, in the open field test oral administration of Hop extracts also prevented an emotional disturbance that appeared in the AD mice at 18 months. Despite lifelong consumption of Hop extracts, no deleterious side effects were observed at any age. These results support the "amyloid hypothesis", and indicate that Hop extract is a promising candidate for an effective prophylactic for AD.

Introduction

Alzheimer Disease (AD) is the most frequently observed neurodegenerative disorder, and more than 1% of people older than 60 years are estimated to be suffering from AD in Japan and other advanced countries [1,2,3]. Several inhibitors for cholinesterase, e.g. donepezil (Aricept®), are available for mitigating clinical phenotypes [4]. However,

these inhibitors are not able to inhibit the progression of neuronal cell death; thus, the long-term prognosis has not appreciably changed [5]. In the brains of AD patients, two major pathologies have been observed, namely Aβ depositions outside the neurons and neurofibrillary tangles within the neurons [1]. Aβ is a small peptide, 40 or 42 amino acids in length, which is derived from APP (amyloid precursor protein) [6] through cleavage by β- and γ-secretases [7,8]. Neurofibrillary tangles are composed of hyper-phosphorylated tau proteins [9].

Several pathological mechanisms have been proposed for AD. Among them, and most widely accepted, is the "amyloid hypothesis", which posits that accumulation/deposition of Aβ is the initial event, which in turn induces neurofibrillary tangles, leading to neuronal dysfunction and neuronal cell death [10,11]. The "amyloid hypothesis" has been supported by several clinical observations [12]. First, the *APP* gene itself, which is located on human chromosome 21, is responsible for one of the familial forms of AD with dominant inheritance [13,14,15], and all the mutated *APP* genes have been shown to produce more Aβ than the normal *APP* gene [16,17]. Two other loci for familial forms of AD with dominant inheritance, on chromosome 1 and 14, have been shown to encode two related proteins, presenilin 1 and 2, respectively, and both are now known to be components of γ-secretase [18]. All identified presenilin mutants from AD patients also produce more Aβ than normal presenilins [17]. Furthermore, a recent cohort study in Iceland identified AD resistant pedigrees. These people possess a novel amino acid substitution (A673T) in APP, near the β-secretase cleavage site, resulting in decreased Aβ production [19].

Based on the "amyloid hypothesis", several strategies to decrease Aβ production/accumulation have been tried, but any clinically successful therapeutic method or drug has not been reported. Even in the brains of healthy individuals, Aβ deposition starts in the forties [20]. It may take 20 years or more to complete the deposition, then another 20 years or more to manifest MCI (mild cognitive impairment), with a wide range of variability [21]. In AD patients, these processes tend to proceed rapidly, eventually leading to "dementia" as early as the fifties, but it is very difficult to predict who will be afflicted by AD before clinical manifestations are observed [22]. Thus, prophylactic drugs for reducing Aβ production, if available, would be best taken as early as the forties, and should be continued for the next several decades. Thus, for such prophylactic drugs, safety and lack of side effects is a critical requirement. From

this perspective, we assumed that plant extracts used in Chinese medicine would be good candidates, because they have been taken by humans for more than a thousand years and are basically safe for humans when administered in moderate doses. In this study, we found that Hop flower extracts partially inhibit Aβ production, and that continuous oral administration of Hop flower extracts ameliorates not only Aβ deposition but also memory and emotional impairments of AD model mice, with no obvious side effects.

Materials and methods

Cell culture and transfection. HEK293A cells were grown at 37 °C in Dulbecco's modified Eagle's medium supplemented with 10% fetal bovine serum. Plasmid transfection was carried out using Lipofectamine plus (Invitrogen), according to the manufacturer's protocol. Cells in a 24-well dish were co-transfected with 200 ng each, of the plasmids pCMX-FLAG-βCTF (wild-type, V717F (Indiana mutation) [14], or V717I (London mutation) [15])-Gal4VP16, pCMX-β-galactosidase, and pTK-(GalRE)x4-Luc [23]. The luciferase values presented in this manuscript were obtained from the transfection of pCMX-FLAG-βCTF(V717F)-Gal4VP16. Hop extracts showed similar inhibitory activities on cells trasfected with the other two constructs (data not shown).

Luciferase and β-galactosidase assays. Twenty-four hours after transfection, different amounts of test compounds in vehicle (DMSO or methanol) or vehicle alone were added to the culture medium, and then incubated for an additional 24 hours. Then, cells were harvested, whole cell extracts were prepared, and luciferase and β-galactosidase assays were carried out, as described previously [24]. The obtained raw luciferase activities were normalized by the β-galactosidase activities to compensate for different transfection efficiencies.

ELISA. To quantify the amounts of Aβ40 and Aβ42, harvested culture media and whole cell extracts were prepared from the transfected HEK293A cells. The culture media was assayed using a human β amyloid (1-40) or (1-42) ELISA kit (WAKO), and the values obtained were normalized by the β-galactosidase activities of the corresponding cell extracts.

Bligh-Dyer method. The Bligh-Dyer method was performed, as described previously [25,26]. Briefly, 100 mg Hop extract was mixed with 3.8 ml of chloroform: methanol: water (1 ml: 2 ml: 0.8 ml). To the resulting mixture, 1 ml of chloroform was added and mixed, and then 1ml of water was added and mixed. The mixture was centrifuged at 1,500 rpm for 10 min. The upper layer (water-soluble fraction: Fraction 1) and the lower layer (lipid-soluble fraction: Fraction 2) were separately collected. Both fractions were dried and weighed. The yields were 23 mg and 76 mg in Fraction 1 and Fraction 2, respectively.

Solid-phase extraction. The dried lipid-soluble fraction (Fraction 2) from the Bligh-Dyer method was dissolved in hexane: chloroform (50:50), and was applied to a Sep-Pak Vac 35 cc (10 g) silica cartridge (Waters). Separation procedures are described in **Figure legends**.

HPLC purification. HPLC was performed using an Alliance 2690 HPLC system (Waters) with columns of COSMOSIL 5CN-MS (10 x 250 mm) (Nacalai Tesque), COSMOSIL 5C18-AR-II (10 x 250 mm) (Nacalai Tesque), Symmetry Shield C18 (4.6 x 250 mm) (Waters), and COSMOSIL π-NAP (4.6 x 250 mm) (Nacalai Tesque). Separation procedures for each column are described in the respective **Figure legends**.

LC/MS analyses. The purified compound was analyzed by LC/MS using a 2795 separation module/Thermo Finnigan, LCQ Deca XP plus (Waters) [27,28].

NMR analysis. NMR analysis was performed using a JNM-LA 500 (JEOL). The values obtained were the following: ^{1}H NMR (500 MHz, $CDCl_3$) δ 4.81-4.76 (m, 3H), 3.64 (m, 1H), 2.93 (dd, J = 14.4, 10.9 Hz, 1H), 2.82 (dd, J = 14.4, 8.0 Hz, 1H), 2.70-2.59 (m, 4H), 1.57 (s, 6H), 1.52 (s, 6H), 1.30 (s, 3H), 1.24 (s, 3H), 1.23 (d, J = 6.3Hz, 3H), 1.21 (d, J = 6.9Hz, 3H); ^{13}C NMR (125MHz, $CDCl_3$) δ 204.8, 202.3, 199.3, 158.1, 135.2, 135.0, 118.1, 117.7, 108.9, 102.3, 92.5, 72.0, 61.8, 39.2, 37.4, 34.9, 26.5, 25.8, 25.7, 25.1, 24.3, 20.1, 18.8, 17.9, 17.7. The calculated value of HRMS (FAB) $C_{25}H_{37}O_5$ [$(M+H)^+$] was 417.2641, and the observed value was 417.2632.